2021

Sustained oxygenation accelerates diabetic wound healing by promoting epithelialization and angiogenesis and decreasing inflammation

Ya Guan

Hong Niu

Zhongting Liu

Yu Dang

Jie Shen

See next page for additional authors

Authors

Ya Guan, Hong Niu, Zhongting Liu, Yu Dang, Jie Shen, Mohamed Zayed, Liang Ma, and Jianjun Guan

HEALTH AND MEDICINE

Sustained oxygenation accelerates diabetic wound healing by promoting epithelialization and angiogenesis and decreasing inflammation

Ya Guan[1†], Hong Niu[1†], Zhongting Liu[1], Yu Dang[1], Jie Shen[2], Mohamed Zayed[3], Liang Ma[4], Jianjun Guan[1]*

Nonhealing diabetic wounds are common complications for diabetic patients. Because chronic hypoxia prominently delays wound healing, sustained oxygenation to alleviate hypoxia is hypothesized to promote diabetic wound healing. However, sustained oxygenation cannot be achieved by current clinical approaches, including hyperbaric oxygen therapy. Here, we present a sustained oxygenation system consisting of oxygen-release microspheres and a reactive oxygen species (ROS)–scavenging hydrogel. The hydrogel captures the naturally elevated ROS in diabetic wounds, which may be further elevated by the oxygen released from the administered microspheres. The sustained release of oxygen augmented the survival and migration of keratinocytes and dermal fibroblasts, promoted angiogenic growth factor expression and angiogenesis in diabetic wounds, and decreased the proinflammatory cytokine expression. These effects significantly increased the wound closure rate. Our findings demonstrate that sustained oxygenation alone, without using drugs, can heal diabetic wounds.

INTRODUCTION

Diabetes is a chronic metabolic disorder affecting 34.2 million people across the United States (*1*). One of the common complications of diabetes is diabetic foot ulcers (DFUs). Roughly 25% of diabetic patients experience DFU (*2*), which causes prolonged pain, decreased vitality, and possibly the need for foot amputation. Conservative medical care for DFU, such as wound off-loading, wound debridement, and infection control (*3*), has inconsistent outcomes and is associated with undesired side effects (*3*, *4*). Stable and safe treatments for chronic, nonhealing diabetic wounds could benefit millions of people.

Cutaneous diabetic wound healing is a complex process with three overlapping phases: inflammation, proliferation, and remodeling (*5*). Immediately after the precipitating injury, impaired vasculature impedes oxygen delivery to the wound, creating a hypoxic environment around the wound (*5*–*7*). This hypoxia is exacerbated by the recruitment of inflammatory cells with high oxygen consumption (*8*, *9*). Although acute hypoxia promotes cell proliferation and initiates tissue repair, long-term oxygen deprivation in chronic wounds impairs the healing process via inhibition of angiogenesis, reepithelialization, and extracellular matrix (ECM) synthesis (*10*). Thus, enhanced wound tissue oxygenation is key to chronic wound healing.

In the past few decades, diabetic wound healing has been clinically facilitated by oxygenation, particularly hyperbaric oxygen therapy (HBOT) (*11*). HBOT delivers 100% oxygen at 2 to 3 atm for 1 to 2 hours per treatment to patients with DFU. In some cases, HBOT promoted diabetic wound healing after 40 or more treatments (*12*, *13*), while in other studies, it did not show beneficial effects (*11*, *14*). Overall, the therapeutic efficacy of HBOT is widely considered to be inconsistent and unsatisfactory (*15*, *16*). This poor performance mainly results from HBOT's inability to continuously provide sufficient oxygen to the wounds because the oxygen content in the poorly vascularized wounds decreases quickly following the treatment (*17*). Moreover, as a systemic oxygen delivery strategy, HBOT may create risks of tissue hyperoxia, such as oxygen toxicity seizure (*17*, *18*).

Several previous reports have developed oxygen-generating systems that are implanted locally to increase the oxygen concentration in wound beds to address the limitations of systemic oxygenation. These oxygen-generating systems were based on H_2O_2 (hydrogen peroxide) (*19*), calcium peroxide (*20*, *21*), and perfluorocarbon (*22*). The localized oxygenation can avoid systemic hyperoxia while accelerating chronic wound healing. However, these oxygenation systems typically release oxygen for only 3 to 6 days (*20*, *22*), which is not long enough for diabetic wound healing. In addition, these systems cannot quickly release sufficient oxygen to relieve hypoxia (*20*, *21*). Oxygen is required for important events, including angiogenesis, granulation, reepithelialization, and ECM synthesis, that often take 2 weeks or longer (*6*, *23*, *24*). Hence, it is critical to develop oxygen-generating systems that continuously oxygenate the wound bed for long periods to accelerate healing.

Here, we present an oxygen-generating system based on oxygen-release microspheres (ORMs) and an injectable, fast-gelling, and reactive oxygen species (ROS)–scavenging hydrogel (ROSS gel). The microspheres quickly release enough oxygen to support cell survival under hypoxia and sustain the release of oxygen for at least 2 weeks. Unlike most current oxygen-generating systems that first release toxic H_2O_2 into the tissue environment and then rely on its decomposition to release oxygen, the designed ORMs directly release oxygen. The injectable and fast-gelling hydrogel is used as a carrier to deliver the microspheres into wounds and quickly immobilize them there, with a high tissue retention rate. The hydrogel has a relatively high water content, enabling it to maintain a moist environment surrounding the wound (*25*). Because it can also scavenge ROS, the oxygen-generating system can capture excessive ROS in diabetic wounds. While ROS play a crucial role in regulating biological and physiological processes,

[1]Department of Mechanical Engineering and Materials Science, Washington University in St. Louis, St. Louis, MO 63130, USA. [2]Department of Orthopedic Surgery, Washington University in St. Louis, St. Louis, MO 63110, USA. [3]Department of Surgery, Section of Vascular Surgery, Washington University in St. Louis, St. Louis, MO 63110, USA. [4]Department of Internal Medicine, Division of Dermatology, Washington University in St. Louis, St. Louis, MO 63110, USA.
*Corresponding author. Email: jguan22@wustl.edu
†These authors contributed equally to this work.

elevated ROS in diabetic wounds can damage cells (*26*, *27*). In this study, we assessed the therapeutic efficacy of the oxygen-generating system in promoting wound closure. We also elucidated the underlying mechanisms of how sustained oxygen release promotes diabetic wound healing. While previous studies have shown that short-term oxygen release facilitated wound closure, the underlying mechanisms were not fully clear and were mainly attributed to wound angiogenesis (*28*). We comprehensively evaluated the effect of sustained oxygen release on skin cell survival, migration, and paracrine effects; intracellular oxygen content; prosurvival pathways; tissue angiogenesis; and tissue inflammation and oxidative stress.

RESULTS

Microspheres released molecular oxygen continuously

The ORMs had a core-shell structure (Fig. 1A), in which the core was a stable polyvinylpyrrolidone (PVP)/H_2O_2 complex. The shell was bioeliminable and bioconjugatable poly(*N*-isopropylacrylamide-co-2-hydroxyethyl methacrylate-co-acrylate-oligolactide-co-*N*-acryloxysuccinimide) [poly(NIPAAm-co-HEMA-co-AOLA-co-NAS)] (fig. S1). The microspheres had a diameter of ~5 μm (Fig. 1B). The core-shell structure was confirmed by fluorescent images (Fig. 1C). The shell of the microspheres was conjugated with catalase to timely convert the H_2O_2 in the released PVP/H_2O_2 into molecular oxygen and keep H_2O_2 from exiting the microspheres and causing toxicity concerns. A layer of catalase was conjugated on the shell, as evidenced by the fluorescence signal of fluorescein isothiocyanate (FITC)–labeled catalase (Fig. 1D).

To determine the oxygen-release kinetics, we used an oxygen-sensitive luminophore, $Ru(Ph_2phen_3)Cl_2$, whose fluorescence intensity is linearly proportional to the oxygen content (*29*, *30*). The ORMs were able to continuously release oxygen during the 2-week experimental period (Fig. 1E). The oxygen level reached above 5% after 2 days of release, and it was maintained above 10% from days 3 to 14. After the 2-week study period, the release medium contained less than 10 μM H_2O_2, as measured by a quantitative peroxide assay kit. This concentration will not cause cell apoptosis (*31*).

Continuous oxygenation of skin cells by released oxygen promoted skin cell survival, migration and paracrine effects, and endothelial lumen formation under hypoxia in vitro

In diabetic wounds, hypoxia is a major factor compromising cell survival and migration, leading to slow wound healing (*6*, *30*, *32*). To evaluate whether oxygen released from ORMs was able to improve cell survival under hypoxia, we incubated human keratinocytes (HaCaT cells), human dermal fibroblasts (HDFs), and human arterial endothelial cells (HAECs) with the ORMs under 1% oxygen. All three cell types exhibited a significantly higher double-stranded DNA (dsDNA; characteristic of live cells) content than the corresponding control groups without ORMs ($P < 0.001$ for HaCaT cells and HAEC and $P < 0.01$ for HDF; Fig. 1, F to H). These results demonstrate that the released oxygen effectively increased skin cell survival under hypoxia. One of the concerns of oxygen treatment is the overproduction of ROS. To characterize ROS expression in the three cell types, we used an ROS-sensitive dye, CM-H_2DCFDA, to stain the cells cultured under normoxia, hypoxia (1% oxygen), and hypoxia with the addition of ORMs (hypoxia/ORM group). The released oxygen in the hypoxia/ORM group substantially increased the ROS level in the three cell types compared to the hypoxia group (Fig. 1, I to K, and figs. S2 to S4). However, the ROS level was similar to the normoxia group ($P > 0.05$ for all cell types). These results, together with dsDNA results, show that the released oxygen did not overproduce ROS and induce cell apoptosis.

To determine whether the released oxygen could increase the migration of keratinocytes and dermal fibroblasts, a scratch assay was performed. After 48 hours of incubation under 1% oxygen, the migration rates of HaCaT cells and HDFs were significantly higher in the ORM groups than in the control groups without ORMs ($P < 0.001$; Fig. 1, L, M, O, and P). These results demonstrate that the released oxygen promoted skin cell migration under hypoxia.

We further elucidated the effect of released oxygen on skin cell expression of angiogenic growth factors under hypoxic conditions. For HaCaT cells, treatment with ORMs significantly increased the expression of vascular endothelial growth factor-A (*VEGFA*; $P < 0.05$) and basic fibroblast growth factor (*FGF2*; $P < 0.001$) (Fig. 1N). For HDFs, the released oxygen significantly augmented the expression of platelet-derived growth factor-B (*PDGFB*; $P < 0.001$) and *FGF2* ($P < 0.001$) (Fig. 1Q). These growth factors play critical roles in reepithelialization and angiogenesis during cutaneous wound healing (*33*–*36*). It remains to be investigated whether the up-regulation of these growth factors is associated with a signaling cascade, which can be activated by the released oxygen.

In chronic wounds, the hypoxic environment impairs angiogenesis, resulting in delayed wound healing (*37*). To evaluate the potential of released oxygen in promoting angiogenesis under hypoxia, we conducted an in vitro endothelial tube formation assay (Fig. 1R). The ORM was injected into three-dimensional (3D) collagen constructs seeded with HAECs. Following 16 hours of culture under 1% oxygen, the HAECs assembled with a significantly greater number of lumens, exhibiting an ~2.5-fold increase in lumen density than the control group ($P < 0.01$; Fig. 1, S and T).

Continuous oxygenation by released oxygen elevated intracellular oxygen content and adenosine triphosphate content and activated extracellular signal–regulated kinase 1/2 and heme oxygenase 1 signaling

To explore how continuous oxygenation by released oxygen increased skin cell survival and migration, we used electron paramagnetic resonance (EPR) to measure the intracellular oxygen content in HaCaT cells (Fig. 2A). After 24 hours of treatment with ORMs under 1% oxygen, the intracellular oxygen content was 2.5 times that of cells without ORM treatment (Fig. 2, B and C). To determine whether the elevated intracellular oxygen content promoted cellular energy production, we measured the intracellular adenosine triphosphate (ATP) level in HaCaT cells. The ATP level in the group treated with ORMs was significantly increased over that in the group without ORM treatment ($P < 0.01$; Fig. 2D), demonstrating that increased cell survival and migration by continuous oxygenation is associated with increased intracellular oxygen content and energy generation.

Oxygen-mediated wound healing is associated with various signaling molecules or pathways, such as mitogen-activated protein kinase (MAPK) (*9*), transforming growth factor–β1 (*38*), heme oxygenase 1 (HO-1) (*39*), and heat shock proteins (*40*). Many researchers have confirmed that HBOT activates MAPK pathway, which modulates cellular responses such as proliferation and migration (*9*). Thus, we investigated whether the ORMs can increase MAPK activity to promote the survival and migration of skin cells. We performed Western blot analysis using HDF to determine

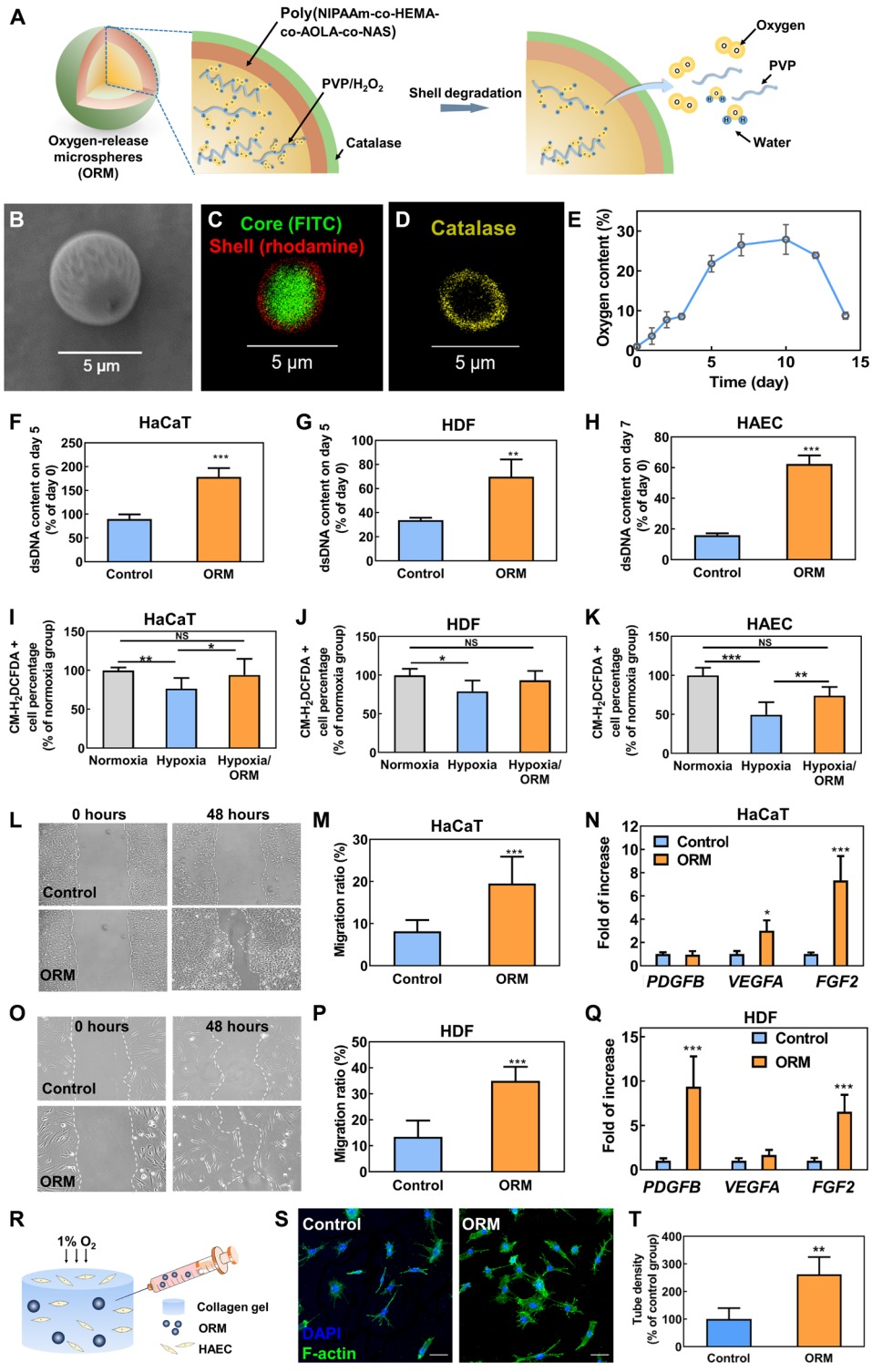

Fig. 1. ORMs continuously release oxygen and regulate skin cell behaviors in vitro. (**A**) Schematic illustration of ORMs and its oxygen-release mechanism. (**B**) Scanning electron microscopy image of ORM. (**C**) Fluorescent image of ORM. (**D**) Fluorescent image of ORM after catalase (labeled with FITC) conjugation. Color of FITC was adjusted. (**E**) Oxygen-release kinetics of ORMs. $n = 8$. (**F** to **H**) Double-stranded DNA (dsDNA) content of HaCaT cells ($n = 5$) (F), human dermal fibroblasts (HDFs; $n = 5$) (G), and human arterial endothelial cell (HAECs; $n = 3$) (H) cultured under hypoxia. (**I** to **K**) ROS content in HaCaT cells ($n = 10$) (I), HDFs ($n = 6$) (J), and HAECs ($n = 8$) (K) cultured under normoxia, hypoxia, or hypoxia with ORM. (**L** and **M**) Migration of HaCaT cells cultured under hypoxia. $n = 4$. (**N**) Gene expression of *PDGFB*, *VEGFA*, and *FGF2* in HaCaT cells cultured under hypoxia. $n \geq 3$. (**O** and **P**) Migration of HDFs cultured under hypoxia. $n = 4$. (**Q**) Gene expression of *PDGFB*, *VEGFA*, and *FGF2* in HDFs cultured under hypoxia. $n \geq 3$. (**R**) Schematic illustration of HAEC tube formation assay. (**S** and **T**) Tube formation (S) and tube density (T) of HAECs cultured under hypoxia for 16 hours. Scale bars, 50 μm. $^*P < 0.05$, $^{**}P < 0.01$, and $^{***}P < 0.001$. NS, not significant; DAPI, 4′,6-diamidino-2-phenylindole.

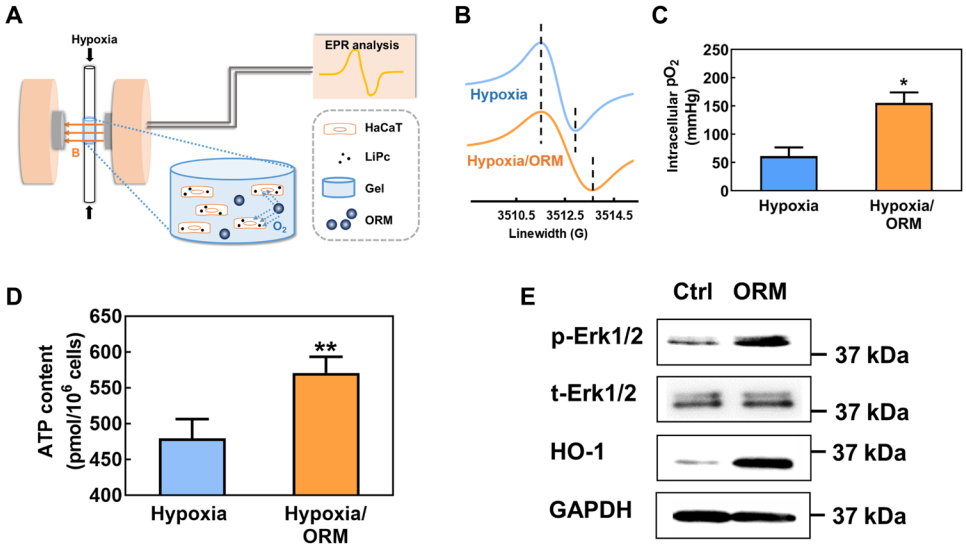

Fig. 2. ORMs elevate intracellular oxygen content and ATP content and activate HO-1 and Erk1/2 pathways under hypoxia. (**A** to **C**) Intracellular oxygen content measured by EPR. Keratinocytes (HaCaT cells) were incubated with lithium phthalocyanine (LiPc) nanoparticles for endocytosis and then cultured under 1% oxygen conditions (with or without ORM) for 24 hours. $n = 3$ for each group. *$P < 0.05$. (**D**) Intracellular ATP content in HaCaT cells measured by an ATP assay kit. Cells were cultured under 1% oxygen conditions (with or without ORM) for 24 hours. **$P < 0.01$. (**E**) Immunoblotting of HO-1 and phosphorylated Erk1/2 (p-Erk1/2) in dermal fibroblasts cultured under hypoxic conditions for 48 hours. t-Erk1/2 was used as the internal reference. Glyceraldehyde-3-phosphate dehydrogenase (GAPDH) served as a loading control.

whether the extracellular signal–regulated kinase (Erk1/2) axis, one of the major cascades of the MAPK pathway, was activated in response to the released oxygen. The results demonstrated that Erk1/2 phosphorylation was increased after the cells were treated with ORMs under 1% oxygen (Fig. 2E). In addition, we investigated whether HO-1, a stress-inducible and cytoprotective protein, was up-regulated after treatment with released oxygen under hypoxia. In the ORM group, the HO-1 expression was more pronounced than in the control group (Fig. 2E). Together, the above results reveal that continuous oxygenation by released oxygen activated the Erk1/2 and HO-1 pathway, leading to enhanced cell survival and migration.

The injectable, thermosensitive, and ROS-scavenging hydrogel delivered ORMs and protected skin cells under oxidative stress

To deliver the ORMs to diabetic wounds and largely retain them in the tissue, we synthesized an injectable and thermosensitive hydrogel with a fast gelation rate. The hydrogel was also designed to capture up-regulated ROS in diabetic wounds to protect skin cells from ROS-induced apoptosis. This hydrogel may also eliminate ROS generated by excessive oxygen release. The hydrogel was synthesized by copolymerizing NIPAAm, HEMA, and 4-(acryloyloxymethyl)-phenylboronic acid pinacol ester (Fig. 3, A and B, and fig. S5). The hydrogel solution [6 weight % (wt%)] had a gelation temperature of 17°C, and it was injectable at 4°C. After being transferred into a 37°C water bath, the hydrogel solution solidified within 6 s (Fig. 3C). The mixture of hydrogel solution and ORMs (40 mg/ml) remained injectable at 4°C and gelled quickly (6 s) at 37°C (Fig. 3C).

The ROS-scavenging capability of the hydrogel was evaluated in terms of its consumption of hydroxyl radical (HO•) and superoxide (O_2•$^-$) and by the hydrogel weight loss induced by H_2O_2. After incubation with HO• for 1 day, the hydrogel scavenged markedly more HO• than the non–ROS-responsive control hydrogel ($P < 0.001$; Fig. 3D). Similarly, the hydrogel eliminated eightfold more O_2•$^-$ than the control hydrogel after incubation for 1 day ($P < 0.001$; Fig. 3E). The hydrogel gradually lost weight in H_2O_2 solution during the 4-week experimental period (Fig. 3F). In contrast, the hydrogel did not show substantial weight loss in Dulbecco's phosphate-buffered saline (DPBS) without H_2O_2.

To evaluate the efficacy of the hydrogel in protecting skin cell survival under pathological oxidative stress, HaCaT cells were seeded on the hydrogel surface in the presence of 100 μM H_2O_2, and the cell viability was quantified (Fig. 3G). The non–ROS-responsive hydrogel was used as a control. We found that HaCaT cells seeded on the hydrogel did not undergo substantial apoptosis in 100 μM H_2O_2 at 48 hours and even proliferated at 72 hours. However, HaCaT cells on the non–ROS-responsive hydrogel had significantly lower viability than the ROS-responsive hydrogel ($P < 0.001$ at 48 and 72 hours), with only ~50% viability at 72 hours (Fig. 3H). These results demonstrate that the ROS-responsive hydrogel was able to protect keratinocytes from apoptosis caused by pathological oxidative stress.

Diabetic wound closure was accelerated by continuous oxygenation and ROS scavenging

To determine whether continuous oxygenation and ROS scavenging can accelerate diabetic wound healing, we administered the hydrogel with ORMs (Gel/ORM group) onto full-thickness excisional wounds on diabetic mice (Fig. 4A). Wounds without treatment (No treatment group) and wounds treated with hydrogel alone (Gel group) were used as controls. The wounds treated with Gel/ORM had a greater closure rate than the No treatment and Gel groups (Fig. 4B). By day 16, the wound size in the Gel/ORM group was reduced to 10.7%, significantly smaller than that in the Gel (30.4%) and No treatment groups (52.2%) ($P < 0.01$; Fig. 4C). Notably, the wound size in the Gel group was substantially smaller than in the No treatment group, demonstrating that the Gel alone promoted wound closure.

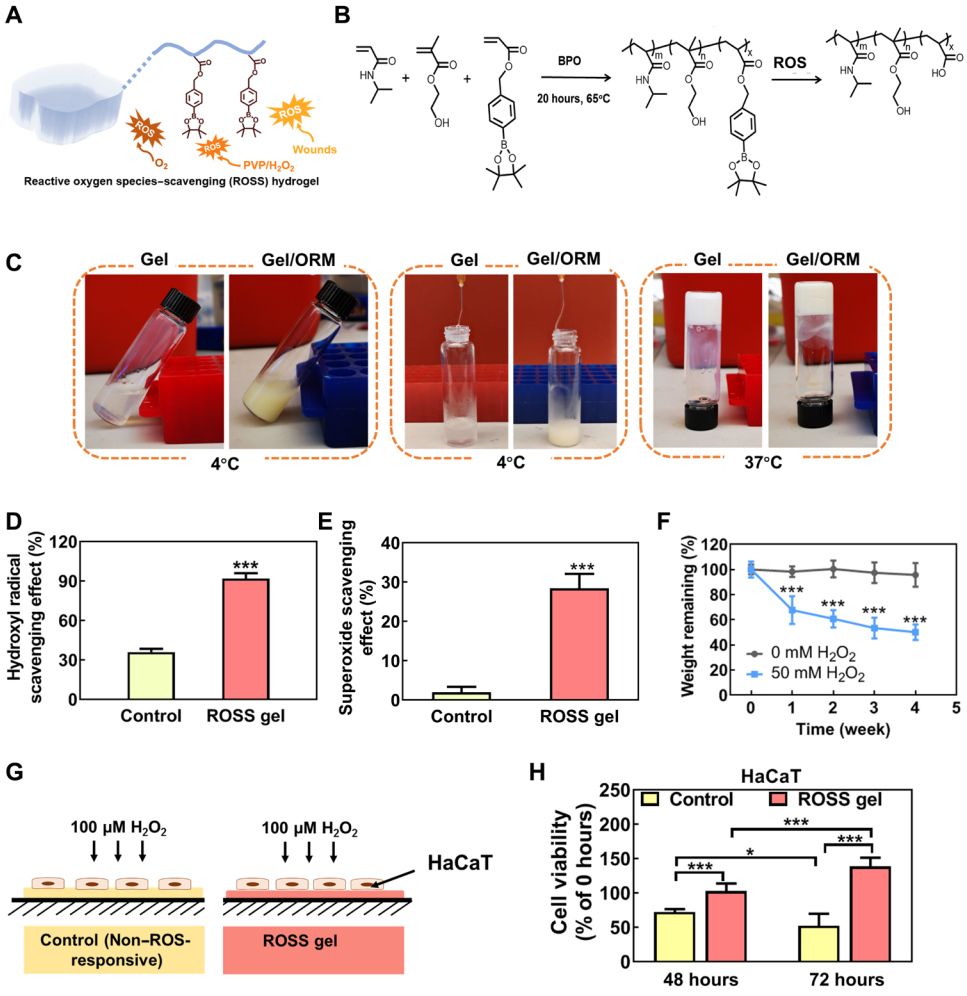

Fig. 3. ROS-scavenging hydrogel protects skin cells under oxidative stress by consuming hydroxyl radicals and superoxides. (**A**) ROS-scavenging (ROSS) hydrogel capable of scavenging ROS in chronic wounds or generated from released oxygen or PVP/H_2O_2. (**B**) Synthesis and ROS-scavenging mechanism of ROSS hydrogel. BPO, benzoyl peroxide. (**C**) Injectability and gelation of ROSS hydrogel (Gel) and Gel/ORM construct. (**D**) Scavenging effect on hydroxyl radicals of ROSS gel and non–ROS-responsive gel (Control) ($n = 4$). (**E**) Scavenging effect on superoxide of ROSS gel and non–ROS-responsive gel (Control) ($n = 3$). (**F**) Degradation of ROSS gel at 37°C for 4 weeks in DPBS with 0 and 50 mM H_2O_2. (**G**) Schematic illustration of an in vitro model for skin cell survival on gels under 100 μM H_2O_2 to mimic the in vivo cell environment under oxidative stress. Non–ROS-responsive gel was used as a control. (**H**) Cell viability of HaCaT cells at 48 and 72 hours on control gel and ROSS gel (normalized to the initial cell viability on each gel). $n \geq 6$. *$P < 0.05$ and ***$P < 0.001$. Photo credit: Hong Niu, Washington University in St. Louis.

Reepithelialization is crucial in wound healing. To evaluate the rate of reepithelialization, we used cytokeratin 14 (K14) and cytokeratin 10 (K10), two markers for basal keratinocytes and spinous keratinocytes, respectively, to stain tissue sections harvested on days 8 and 16. On day 8, in the Gel/ORM group, the wound gap was nearly enclosed by a complete layer of basal keratinocytes ($K14^+$), while in the No treatment and Gel groups, keratinocyte migration was much slower (Fig. 4D and fig. S6). In addition, compared to the No treatment and Gel groups, the Gel/ORM group formed a more mature spinous layer composed of $K10^+$ keratinocytes. On day 16, the migration of basal keratinocytes was complete, and proliferation and differentiation were ongoing in the No treatment and Gel groups. In contrast, reepithelialization was fully complete in the Gel/ORM group, as evidenced by a clear stratified epithelium (Fig. 4D and fig. S6). On both day 8 and day 16, K14 staining of the hair follicles in the basal layer of the epidermis (Fig. 4E) revealed a significantly increased hair follicle density in the Gel/ORM group than in the No treatment and Gel groups ($P < 0.01$; Fig. 4F). These results demonstrate that the continuous oxygenation by released oxygen, together with ROS scavenging, effectively accelerated keratinocyte migration and hair follicle formation, consequently promoting reepithelialization of the diabetic wounds.

Epidermal thickness, another indicator of wound healing, increases during the initial inflammatory and proliferative stages and then decreases during the remodeling stage (*41*). On day 8, the wounds treated with Gel/ORM exhibited the thickest epidermis. By day 16, it had become the thinnest ($P < 0.001$; Fig. 4, G and H), suggesting that the continuous oxygenation and ROS scavenging facilitated the wound's healing progressions from the inflammatory and proliferative stages to the remodeling stage.

To determine whether the accelerated wound closure was associated with scar formation, we performed picrosirius red staining for collagens in the wounds. On day 16, the Gel/ORM group had a significantly lower total collagen content than the No treatment

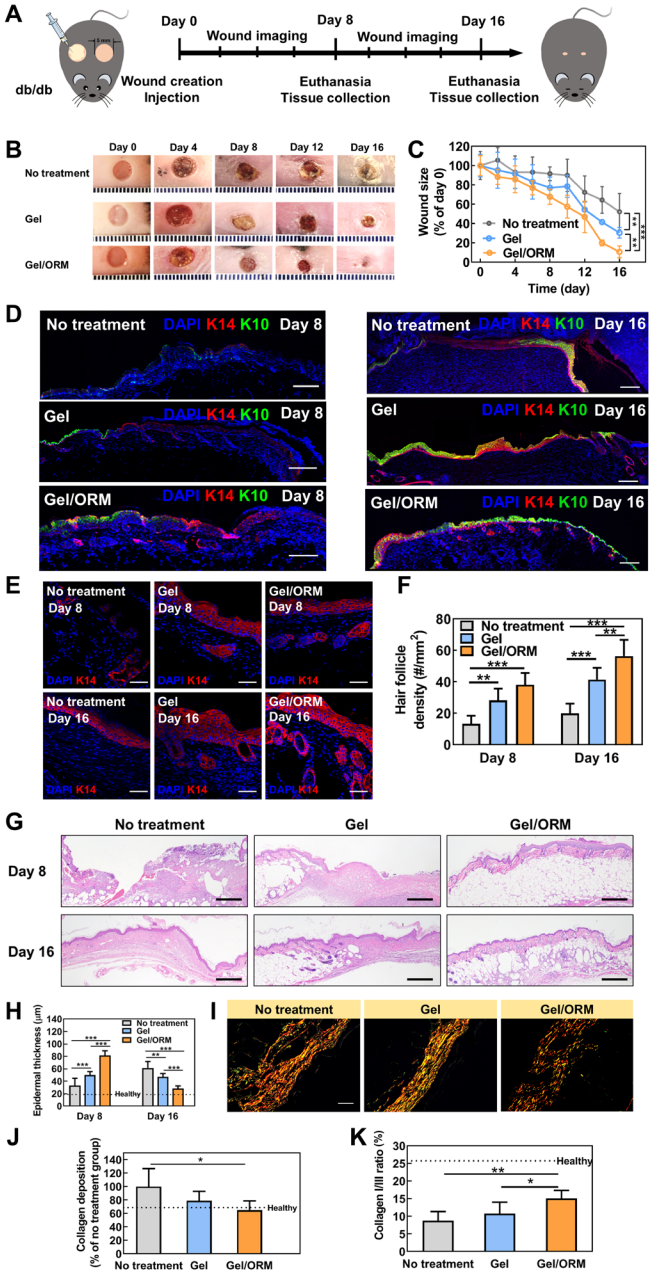

Fig. 4. ORMs encapsulated in ROS-scavenging hydrogel accelerate wound healing in db/db mice. (**A**) Schematic illustration of the design of animal experiments to test the therapeutic effect of ROSS gel (Gel) and ORMs in a db/db mouse model. (**B**) Representative images of the wounds treated with or without Gel and ORMs for 16 days. (**C**) Wound size change during 16 days of post wounding. Wound size at each time point was normalized to day 0. $n \geq 8$. (**D**) Immunofluorescence staining of cytokeratin 10 (K10, green) and cytokeratin 14 (K14, red) for the wounds at days 8 and 16. Scale bars, 200 μm. (**E**) Immunofluorescence staining of K14 (red) in the wounded region at days 8 and 16. Scale bars, 50 μm. (**F**) Quantification of hair follicle density in the wounded region at days 8 and 16. (**G**) Hematoxylin and eosin staining of the wounded skin at days 8 and 16. Scale bars, 500 μm. (**H**) Quantification of epidermal thickness. Epidermal thickness was calculated in the region where wound was closed. (**I**) Picrosirius red staining of the wounded skin at day 16. Scale bar, 50 μm. (**J**) Quantification of total collagen deposition at day 16. (**K**) Quantification of collagen I/III ratio at day 16. *$P < 0.05$, **$P < 0.01$, and ***$P < 0.001$. Photo credit: Ya Guan and Hong Niu, Washington University in St. Louis.

group ($P < 0.05$; Fig. 4, I and J). In addition, a significantly higher collagen I/III ratio was found for the Gel/ORM group than the No treatment and Gel groups ($P < 0.05$; Fig. 4K). Compared to the control groups, this collagen I/III ratio was closer to that of uninjured skin. The reduced collagen deposition and higher collagen I/III ratio demonstrate that the enhanced wound healing did not induce scar formation (*42*, *43*).

Continuous oxygenation and ROS scavenging in diabetic wounds promoted cell proliferation and metabolism

To understand the role of continuous oxygenation and ROS scavenging in diabetic wound healing at the cellular level, we examined cell proliferation and metabolism in the wounds. Compared to the No treatment group on both day 8 and day 16, the ROS-scavenging activity of the hydrogel alone had significantly increased the density of $Ki67^+$ proliferating cells. On day 16, the density of proliferating cells treated with Gel/ORM had increased further (Fig. 5, A and C). Continuous oxygenation and ROS scavenging also increased the skin cell metabolic rate, as judged by the peroxisome proliferator–activated receptor gamma coactivator 1 α (PGC1α) positive cell density (Fig. 5, B and D) (*44*). Compared with the No treatment group, the Gel group exhibited a significantly higher density of $PGC1\alpha^+$ cells. The release of oxygen in the Gel/ORM group further increased the $PGC1\alpha^+$ cell density at both time points.

Continuous oxygenation and ROS scavenging in diabetic wounds stimulated angiogenic growth factor expression and angiogenesis

To determine whether continuous oxygenation and ROS scavenging affect the expression of angiogenic growth factors in diabetic wounds, real-time reverse transcription polymerase chain reaction (RT-PCR) was performed using wound tissues extracted 8 days after surgical wounding (Fig. 5, E and F). Among different angiogenic growth factors, *Pdgfb* expression was significantly increased in both the Gel and Gel/ORM groups ($P < 0.01$; Fig. 5E), with the Gel/ORM group showing substantially greater expression than the Gel group ($P > 0.05$). Notably, the Gel/ORM group exhibited significantly higher *Vegfa* expression than the Gel and No treatment groups ($P < 0.01$; Fig. 5F).

To evaluate whether continuous oxygenation and ROS scavenging stimulated angiogenesis in the diabetic wounds, we quantified the capillary densities in the Gel/ORM, Gel, and No treatment groups at middle stage (day 8) and late stage (day 16) of the wound healing. At both stages, the Gel group had a significantly higher density of capillaries than the No treatment group, demonstrating that ROS scavenging promoted diabetic wound angiogenesis (Fig. 5, G and H). The simultaneous ROS scavenging and continuous oxygenation in the Gel/ORM group further significantly stimulated angiogenesis (Fig. 5, G and H).

Continuous oxygenation and ROS scavenging in diabetic wounds alleviated oxidative stress, inflammation, and proinflammatory cytokine expression

The ROS-scavenging hydrogel decreased the ROS content in diabetic wounds (Fig. 6, A and C). On both day 8 and day 16, the ROS^+ cell density was markedly lower in the Gel group than in the No treatment group ($P < 0.001$). Although the continuous oxygenation of the diabetic wounds may have led to the formation of ROS, the hydrogel was able to capture it. On days 8 and 16, the Gel and Gel/ORM

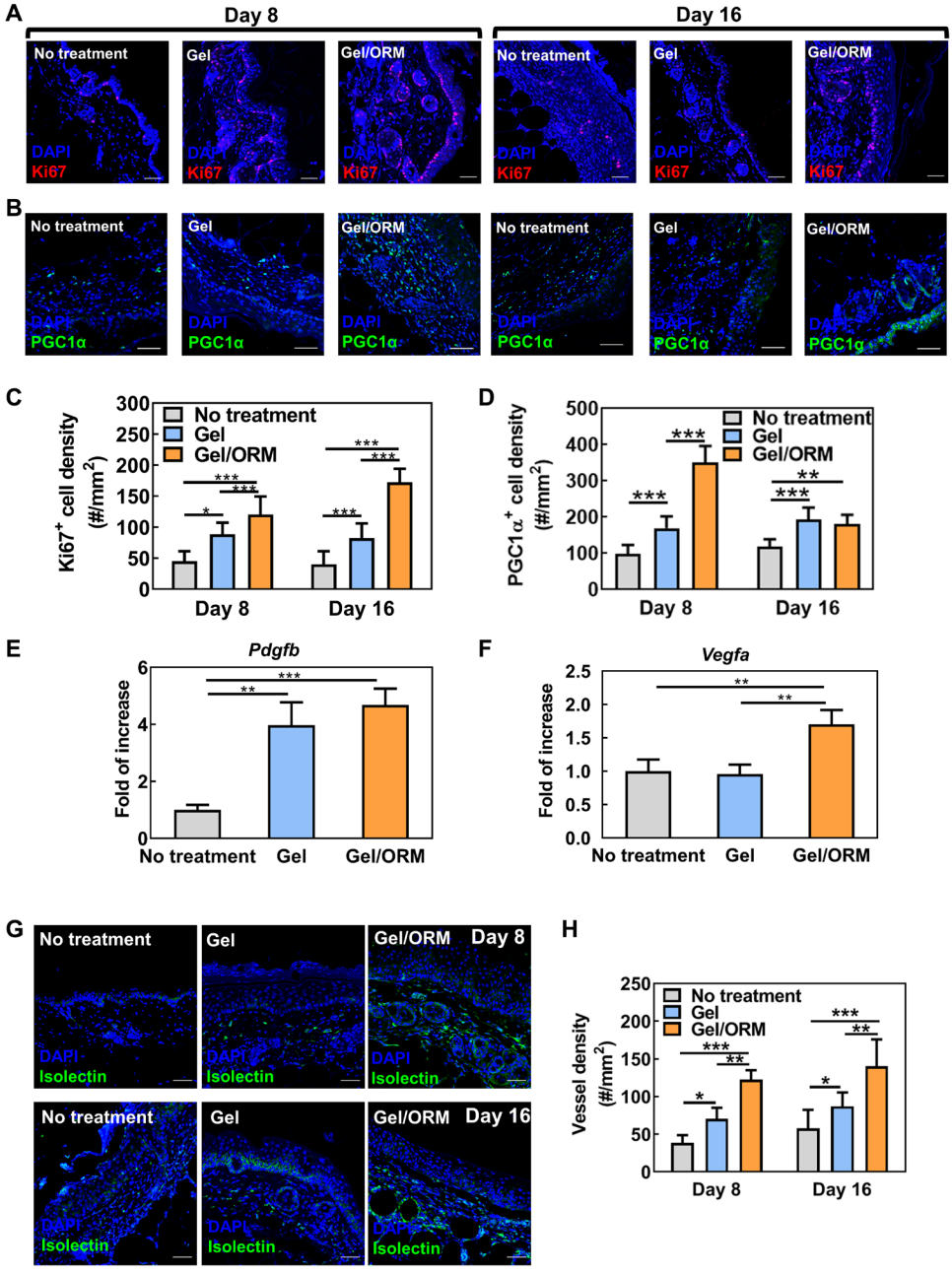

Fig. 5. Continuous oxygenation and ROS scavenging promote cell proliferation and metabolism and stimulate angiogenic growth factor expression and angiogenesis in diabetic wounds. (**A**) Immunofluorescence staining of Ki67 (red) in the wounded region at 8 and 16 days after wounding. Scale bars, 50 μm. (**B**) Immunofluorescence staining of PGC1α (green) in the wounded region at 8 and 16 days after wounding. Scale bars, 50 μm. (**C**) Quantification of Ki67$^+$ cell density. (**D**) Quantification of PGC1α$^+$ cell density. (**E** and **F**) Gene expression of *Pdgfb* (E) and *Vegfa* (F) from the tissue lysates extracted from the wounded skin at day 8. $n \geq 4$. (**G**) Immunofluorescence staining of isolectin (green) in the wounded region at 8 and 16 days after wounding. Scale bars, 50 μm. Nuclei were stained with DAPI in all immunofluorescence staining images. (**H**) Quantification of vessel density. *$P < 0.05$, **$P < 0.01$, and ***$P < 0.001$.

groups showed similar densities of ROS$^+$ cells ($P > 0.05$; Fig. 6, A and C), demonstrating that the hydrogel can efficiently scavenge ROS even if continuous oxygenation induces ROS formation.

To elucidate the impact of continuous oxygenation and ROS scavenging on the inflammatory response in diabetic wounds, we evaluated inflammatory cell density in the tissue by CD86 staining. The CD86$^+$ inflammatory cell density in the Gel and Gel/ORM groups was significantly lower than in the No treatment group (with $P < 0.001$ on day 8 and $P < 0.05$ on day 16; Fig. 6, B and D). Notably, the Gel and Gel/ORM groups had similar inflammatory cell densities. These results demonstrate that ROS scavenging by the hydrogel decreased diabetic wound inflammation.

To further reveal the role of released oxygen in tissue inflammation, we assessed proinflammatory cytokine expressions in diabetic wounds (Fig. 6, E and F). Compared with the Gel group, the Gel/ORM group exhibited reduced expression of various proinflammatory

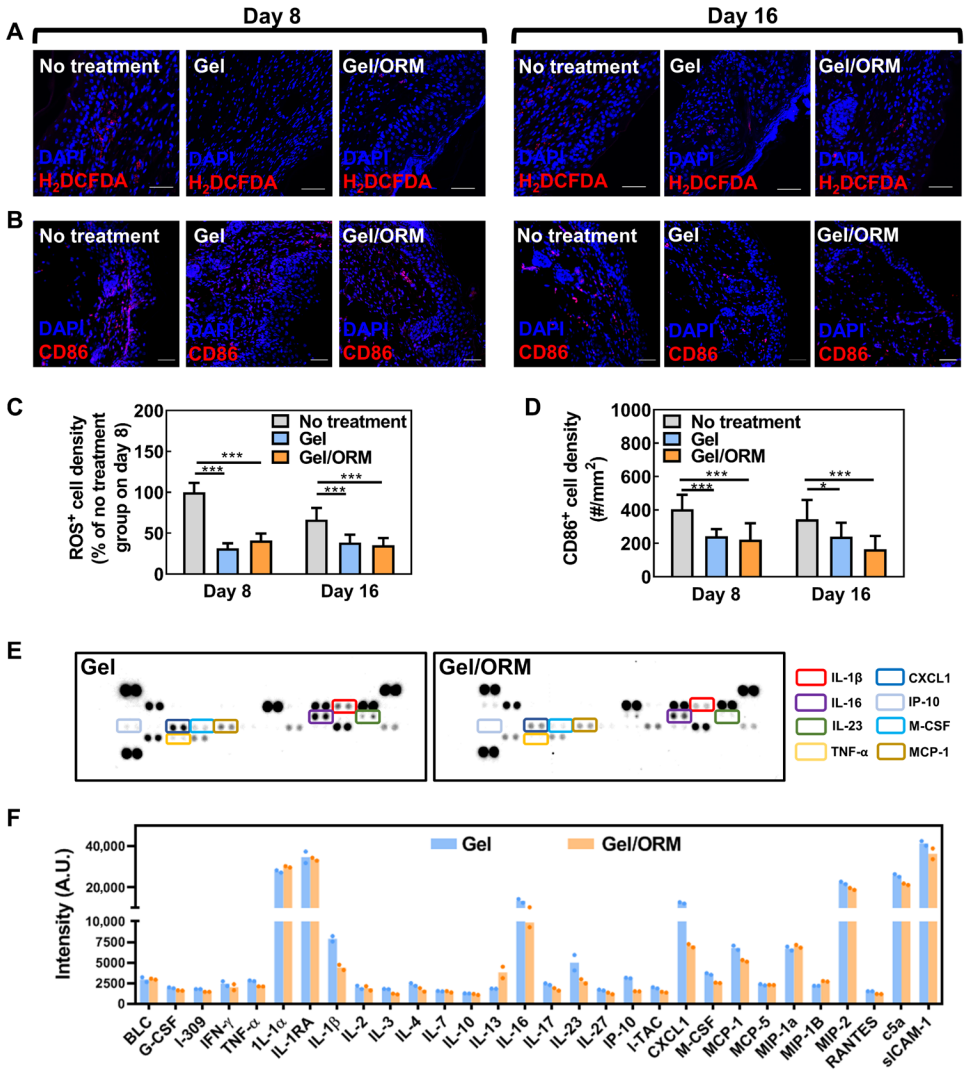

Fig. 6. Continuous oxygenation and ROS scavenging alleviate oxidative stress, inflammation, and proinflammatory cytokine expression in diabetic wounds. (**A**) Immunofluorescence staining of CM-H_2DCFDA (red) at the wounded site at days 8 and 16. Scale bars, 50 μm. (**B**) Immunofluorescence staining of CD86 (red) at the wounded site at days 8 and 16. Scale bars, 50 μm. Nuclei were stained with DAPI in all immunofluorescence staining images. (**C**) Quantification of ROS^+ cell density. The results were normalized to the ROS^+ cell density in No treatment group at day 8. $n \geq 8$. (**D**) Quantification of $CD86^+$ cell density. $^*P < 0.05$ and $^{***}P < 0.001$. (**E**) Cytokine array analysis of the proinflammatory cytokine level in the wounds 8 days after treatment. (**F**) Quantitative summary of cytokine array analysis in (E). A.U., arbitrary units.

cytokines, such as interleukin-1β (IL-1β), tumor necrosis factor–α (TNF-α), interferon-γ (IFN-γ), and chemokine ligand 1(CXCL1). These results suggest that continuous oxygenation has the potential to decrease inflammation during diabetic wound healing.

Continuous oxygenation in diabetic wounds up-regulated phosphorylated Erk1/2 and HO-1 expressions

After showing that the oxygenation of keratinocytes by released oxygen up-regulated phosphorylated Erk1/2 (p-Erk1/2) and HO-1 expressions in vitro, we next evaluated whether continuous oxygenation up-regulated these expressions in diabetic wounds. Consistent with the in vitro findings, the p-Erk1/2 and HO-1 expressions were substantially up-regulated in the Gel/ORM group on days 8 and 16 (Fig. 7).

DISCUSSION

Chronic hypoxia is a main characteristic of diabetic wounds and a severe impediment to the healing process. Consequently, sustained oxygenation of skin cells to mitigate chronic hypoxia represents an approach to accelerating diabetic wound healing. Oxygen therapy is advantageous over drug therapy because it raises fewer toxicity concerns (*45*). However, current oxygen therapy approaches cannot provide sufficient oxygen to metabolic-demanding skin cells long enough to promote diabetic wound healing (*46*–*48*). In this work, we developed an oxygen-release system that continuously oxygenates diabetic wounds. It is composed of ORMs and their carrier, an injectable, thermosensitive, fast-gelling, and ROS-scavenging hydrogel. The ORMs have a core-shell structure, with PVP/H_2O_2 complex as the core and a bioeliminable polymer as the shell. The high–molecular

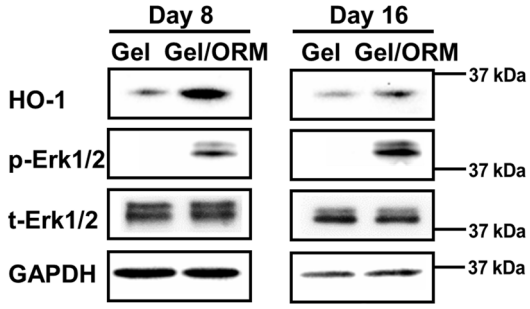

Fig. 7. ORMs activate HO-1 and Erk1/2 pathways. Immunoblotting of HO-1 and p-Erk1/2 from the tissue lysates extracted from wounded skin at days 8 and 16 after wounding. t-Erk1/2 was used as the internal reference. GAPDH was used as a loading control.

weight PVP/H_2O_2 complex reduces H_2O_2 diffusivity, allowing for sustained release of H_2O_2 during the hydrolysis of the shell polymer (*49*, *50*). The ORM surface is conjugated with catalase to timely convert H_2O_2 in the released PVP/H_2O_2 into molecular oxygen (Fig. 1A). Therefore, the ORMs can directly release oxygen (Fig. 1E), whereas most other oxygen-release systems directly release H_2O_2 instead of oxygen (*20*, *51*, *52*). We demonstrated that the microspheres could release oxygen for at least 2 weeks (Fig. 1E), longer than most other oxygen-release systems (*20*, *22*). The injectable, thermosensitive, and fast-gelling hydrogel used as the ORM carrier largely retained the ORMs in the diabetic wounds after delivery. The ROS-scavenging hydrogel both eliminates the H_2O_2 in the released PVP/H_2O_2, even if it is not completely converted by catalase, and captures the up-regulated H_2O_2 in diabetic wounds to decrease oxidative stress and accelerate wound healing. To the best of our knowledge, no current oxygen-release system has been designed to release molecular oxygen and scavenge ROS simultaneously.

We evaluated the efficacy and mechanism of action of the oxygen-release system in healing excisional wounds in db/db mice (Fig. 4A). This model exhibits significant delay in wound closure and impaired wound bed vascularization compared with other well-accepted murine diabetes models, such as streptozocin-induced C57BL/6J and Akita mice (*53*). Our results showed that the oxygen-release system substantially promoted wound closure (Fig. 4C). More specifically, we sought to demonstrate that the accelerated wound healing was caused by the sustained oxygenation and ROS scavenging in diabetic wounds that augmented cell survival, accelerated cell migration, stimulated angiogenesis, and reduced oxidative stress and inflammation (Fig. 8).

First, we investigated the effect of oxygen released from ORMs on skin cell survival in a hypoxic environment. We conducted in vitro studies under 1% O_2 and high-glucose conditions to mimic the in vivo microenvironment in diabetic wounds (*8*, *54*). The survival of keratinocytes, fibroblasts, and endothelial cells under hypoxia was significantly increased with the supplement of oxygen released from the ORMs (Fig. 1, F to H). These three cell types are responsible for epithelialization, wound contraction, and angiogenesis. In diabetic wounds, treatment with the oxygen-release system significantly increased the density of proliferating cells (Fig. 5, A and C). The augmented cell survival can be attributed to the elevated cellular oxygen content (Fig. 2C). Cellular oxygen is essential for mitochondrial metabolism, and the low oxygen level in diabetic wounds impairs this process (*55*). The release of oxygen significantly increased the mitochondrial metabolism of the cells in the wounds on day 8, as evidenced by greater PGC1α^+ cell density (Fig. 5, B and D). Mechanistically, we found that the enhanced skin cell survival with released oxygen is associated with the up-regulation of p-Erk1/2 in vitro and in vivo (Figs. 2E and 7).

Next, we demonstrated that continuous oxygenation of skin cells promoted the migration and paracrine effects of keratinocytes and fibroblasts under hypoxia (Fig. 1, L to Q). The migration of these cells is essential for the regeneration of the epidermis and dermis. The enhanced paracrine effects, in terms of up-regulation of growth factors such as *VEGFA*, *FGF2*, and *PDGFB*, facilitate the regeneration. Specifically, *VEGFA* and *FGF2* have been found to increase keratinocyte migration and proliferation (*56*–*59*). The up-regulated expression of *VEGFA*, *FGF2*, and *PDGFB* in skin cells in response to released oxygen may be attributed to increased p-Erk1/2 expression (Fig. 2E). Previous studies have demonstrated that activation of Erk1/2 pathway was able to up-regulate cell angiogenic growth factor expression (*60*–*62*). The enhanced keratinocyte survival, migration, and paracrine effects of continuous oxygenation led to a significant increase in the wound closure rate (Fig. 4C) and formation of a stratified epithelium (Fig. 4D).

Angiogenesis in diabetic wounds is essential for the regeneration of the dermis. Although acute hypoxia induces angiogenesis mediated by hypoxia-inducible transcription factors, chronic oxygen deprivation cannot sustain this process, thereby impairing the healing process (*6*). We found that the released oxygen increased endothelial cell survival (Fig. 1H) and tube formation (Fig. 1, R to T) in vitro. In diabetic wounds, the continuous oxygenation significantly stimulated capillary formation (Fig. 5, G and H). The quicker angiogenesis may also be attributed to the enhanced paracrine effects because the expressions of angiogenic growth factors *Pdgfb* and *Vegfa* were substantially up-regulated (Fig. 5, E and F).

Furthermore, we showed that the developed oxygen delivery system alleviated oxidative stress in diabetic wounds (Fig. 6, A and C). The decreased oxidative stress was due to the ROS-scavenging hydrogel since the ROS$^+$ cell densities in the Gel and Gel/ORM groups were similar. This result minimizes potential concern that oxygen release may lead to ROS overproduction. The decreased oxidative stress may also be associated with increased HO-1 expression under hypoxic conditions (Figs. 2E and 7). HO-1 has antioxidant effects and has been reported to promote diabetic wound healing (*63*, *64*).

Last, we showed that the oxygen-release system reduced inflammation in diabetic wounds (Fig. 6, B and D). Chronic wounds are characterized by a high concentration of proinflammatory cells, the major contributor of proinflammatory cytokines, such as TNF-α, IL-1β, and CXCL1 (*65*). In addition, hyperglycemia exacerbates inflammatory stress via the production of proinflammatory cytokines such as TNF-α (*66*). Our results show that ROS-scavenging hydrogel greatly decreased the number of inflammatory cells (Fig. 6, B and D) and the released oxygen further reduced the expression of major proinflammatory cytokines (Fig. 6, E and F). Future studies will focus on delineating signaling pathways as the underlying mechanism in suppressing inflammation by sustained oxygen release in diabetic wounds.

Overall, we demonstrate in this report that a sustained oxygen-release system that simultaneously scavenges ROS substantially accelerated diabetic wound closure. The sustained release of oxygen had multiple effects: It promoted skin cell survival, migration, and paracrine effects; stimulated endothelial tube formation and angiogenesis;

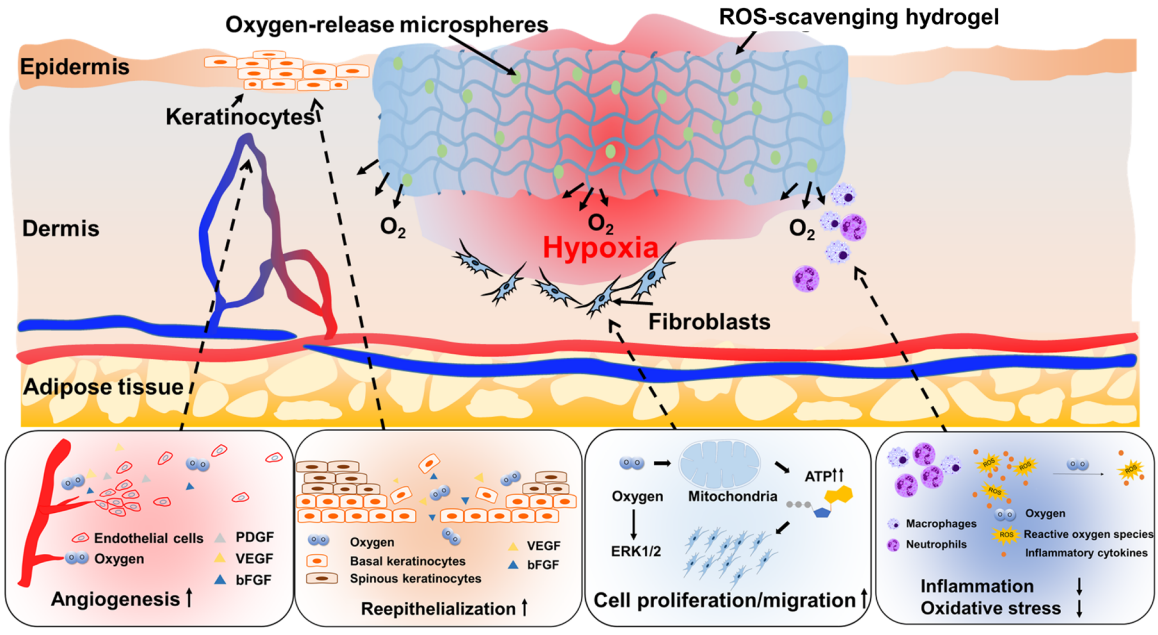

Fig. 8. Mechanisms of accelerated wound healing by ORMs encapsulated in ROS-scavenging hydrogel. The ORMs and ROSS gel augmented cell proliferation and migration, promoted angiogenesis and reepithelialization, and decreased inflammation and oxidative stress in diabetic wounds.

and decreased tissue inflammation. Compared with the results of previous studies using growth factors or exogenous cells to treat impaired wound healing in the same animal model, our oxygen-release system exhibited faster (*67*–*69*) or similar wound closure rates (*70*, *71*). Thus, it represents an effective therapeutic approach for accelerated healing of chronic diabetic wounds without using drugs. Beyond wound healing, the developed oxygen-release system may be used to treat other ischemic diseases, such as peripheral artery disease and coronary heart disease. Given the limitations of rodent models in illustrating more complex human pathophysiology, we will further test our oxygen-release system in large animals and optimize the oxygen-release kinetics and ROS-scavenging capability accordingly.

MATERIALS AND METHODS

Materials

All chemicals were purchased from MilliporeSigma unless otherwise stated. NIPAAm (TCI) was recrystallized in hexane before use. HEMA (Alfa Aesar) was used before passing through a column filled with inhibitor removers. Benzoyl peroxide (BPO; Thermo Fisher Scientific), acryloyl chloride, 4-(hydroxymethyl)-phenylboronic acid pinacol ester, triethylamine (Fisher Scientific), PVP (40 kDa; Fisher Scientific), hydrogen peroxide solution (30%), and bovine liver catalase (2000 to 5000 U/mg) were used as received.

Synthesis and characterization of ROS-scavenging hydrogel

4-(acryloxymethyl)-phenylboronic acid pinacol ester was synthesized by the reaction between acryloyl chloride and 4-(hydroxymethyl)-phenylboronic acid pinacol ester (*72*). The ROS-scavenging hydrogel was synthesized by free radical polymerization of NIPAAm, HEMA, and 4-(acryloxymethyl)-phenylboronic acid pinacol ester using BPO as initiator and 1,4-dioxane as solvent. The reaction was conducted at 70°C overnight with the protection of nitrogen. The polymer solution was precipitated in hexane. The polymer was purified twice by dissolving in tetrahydrofuran and precipitating in ethyl ether. The polymer was dissolved in DPBS at 4°C to make a 6 wt% solution. The injectability of the 4°C solution with or without ORMs (40 mg/ml) was tested by a 26-gauge needle (*73*, *74*).

Hydrogel H_2O_2 responsiveness was characterized by its weight loss after being incubated in H_2O_2 solution for 4 weeks. Briefly, the hydrogel solution was solidified in 1.5 ml microcentrifuge tubes at 37°C. After the supernatant was discarded, 0.2 ml, 37°C DPBS with or without 50 mM H_2O_2 was added. The samples were collected at predetermined time points and freeze-dried. The weight loss was calculated. To determine scavenging capability of the hydrogel for hydroxyl radicals and superoxide, Fenton reaction assay (*75*) and pyrogallol assay (*76*) were performed, respectively. Briefly, for Fenton reaction assay, hydrogel solution or deionized (DI) water (control group) was incubated with $FeSO_4$, safranin O, and H_2O_2 for 5 min, followed by heating at 55°C for 30 min. After the samples were cooled to room temperature, the absorbance was measured at 492 nm using a microplate reader. For pyrogallol assay, the hydrogel solution or DI water was mixed with tris-HCl. Pyrogallol solution (3 mM) was then added dropwise in the dark. The reaction was terminated by adding 8 M HCl. The absorbance was acquired at 299 nm.

Cell survival on ROS-scavenging hydrogel in the presence of H_2O_2

The ROS-scavenging hydrogel was plated on 96-well plates. HaCaT cells (AddexBio) were seeded on the hydrogel surface at a density of 50,000 per well in optimized Dulbecco's modified Eagle's medium (DMEM, AddexBio) with 5% fetal bovine serum (FBS) and 1% penicillin-streptomycin. After 24 hours of culture, the medium was discarded. A total of 200 μl of 100 μM H_2O_2-containing medium was added to each well. At 48 and 72 hours, the viability of HaCaT was measured by MTT assay. The non–ROS-responsive hydrogel,

poly(NIPAAm-co-HEMA-co-acrylate-oligolactide), was used as a control (*50*, *74*).

Fabrication of ORMs and catalase conjugation

The ORMs were fabricated by double emulsion method. Briefly, the shell of the microspheres was synthesized by the copolymerization of NIPAAm, HEMA, NAS, and AOLA. The chemical structure of the shell polymer was confirmed by ^{1}H-NMR (proton nuclear magnetic resonance) (fig. S1). The synthesized polymer was dissolved in dichloromethane to form the 5 wt% oil phase. The inner water phase was prepared by dissolving 242 mg of PVP in 1 ml, 30% H_2O_2 at 4°C overnight. The water phase was rapidly added into the oil phase and sonicated by an ultrasonic liquid processor (Cole Parmer). The primary water-in-oil emulsion was then poured into poly(vinyl alcohol) solution to form the water-in-oil-in-water double emulsion. The mixture was stirred for 3 hours to remove dichloromethane, followed by centrifugation to collect the microspheres. Morphology and size of the microspheres were characterized by scanning electron microscopy images. To confirm the core-shell structure, FITC and rhodamine were added to the PVP/H_2O_2 solution and polymer/dichloromethane solution, respectively. The fluorescent images were acquired by a confocal microscope. To conjugate catalase onto the microsphere shell, 40 mg microspheres were mixed with 6 ml catalase solution (5 mg/ml in DI water) and stirred for 4 hours at 4°C. The mixture was then centrifuged. The microspheres were washed three times with DI water to remove unconjugated catalase. To confirm the conjugation, the catalase was prelabeled by FITC, and the fluorescent images of the microspheres were taken after the conjugation.

Oxygen-release kinetics

The ROS-sensitive hydrogel was dissolved in 4°C DPBS to make a 6 wt% solution. The ORMs were then mixed with the hydrogel solution at a concentration of 40 mg/ml. The oxygen-release kinetics was determined by our established method (*50*, *74*, *77*). The wells of a 96-well plate were covered by a polydimethylsiloxane membrane loaded with an oxygen-sensitive luminophore $Ru(Ph_2phen_3)Cl_2$ and an oxygen-insensitive dye rhodamine B. Two hundred microliters of the mixture was then added into each well ($n = 8$ for each group). After gelation at 37°C, the supernatant was removed. A total of 200 μl of DPBS preincubated in 1% oxygen condition was added. The oxygen-release study was performed in 1% oxygen and 37°C conditions for 2 weeks. At each time point, the fluorescent intensity for $Ru(Ph_2phen_3)Cl_2$ was measured (emission at 610 nm and excitation at 470 nm). The fluorescent intensity for rhodamine was also determined (emission at 576 nm and excitation at 543 nm) and used for normalization. Oxygen concentration was determined by the calibration curve.

Cell survival, migration, and ROS content under hypoxia

HaCaT cells (AddexBio) were cultured in optimized DMEM (AddexBio) with 5% FBS and 1% penicillin-streptomycin. HDF (Lonza) were cultured in FGM-2 BulletKit (Lonza). HAEC (Cell Systems) were cultured in EGM-2 BulletKit (Lonza). The medium was changed every other day.

For all in vitro studies, cells were cultured using high-glucose (450 mg/dl) and serum-free medium under 1% oxygen and 37°C conditions. To determine cell survival, the cells were cultured in a 96-well plate using medium with or without ORMs (40 mg/ml, $n \geq 5$ for each group). The dsDNA content was measured using PicoGreen dsDNA assay kit (Invitrogen) after 5 days of culture for HaCaT cells and HDFs and after 7 days of culture for HAEC.

To perform cell migration assay, the cells were first cultured in a six-well plate to reach 85 to 95% confluency ($n = 4$ for each group). The monolayer was then scraped with a 200 μl pipette tip, washed, and supplemented with serum-free medium with or without ORMs (40 mg/ml). After 48 hours, optical images were taken using an optical microscope (Olympus IX70). The distances between two sides of the scratch were measured using ImageJ. The migration ratio was calculated as

$$\text{migration ratio} = \frac{\text{Interval at 0 hour} - \text{interval at 48 hours}}{\text{Interval at 0 hour}} \times 100\%$$

To measure intracellular ROS content, the cells were prestained with ROS-sensitive dye CM-H_2DCFDA and cultured with serum-free medium with or without ORMs (40 mg/ml). After 3 days of culture for HaCaT cells and HAEC and 5 days of culture for HDF, the cells were fixed and stained with 4′,6-diamidino-2-phenylindole (DAPI). Fluorescent images were taken using a confocal microscope. The CM-H_2DCFDA positive cell density was quantified from at least 10 images for each group and then normalized to the CM-H_2DCFDA positive cell density cultured under normoxia.

Measurement of intracellular oxygen content

To determine the intracellular oxygen content, HaCaT cells were incubated with lithium phthalocyanine nanoparticles for 2 hours to allow cellular uptake. The residual nanoparticles were washed with DPBS three times. After trypsinization, the cells were encapsulated in the ROS-sensitive hydrogel or mixture of hydrogel and ORMs (40 mg/ml). The samples were transferred into EPR tubes (Wilmad-LabGlass, $n = 3$ for each group). The EPR tubes were opened on both sides and placed in a hypoxic incubator (1% oxygen, 37°C) for 4 hours for complete gelation and gas balance. After that, the tubes were sealed and incubated for 24 hours under 1% oxygen. The EPR spectrum was recorded using an X-band EPR instrument (Bruker). The parameters used in this experiment were 0.1 mW for microwave power, 1.0 dB for attenuation, and 9.8 GHz for frequency, following our reported method (*77*, *78*). Oxygen partial pressure (pO_2) was calculated from the linewidth of the spectrum and calibration curve of linewidth versus oxygen concentration.

Measurement of intracellular ATP level

To determine the intracellular ATP level, HaCaT were cultured in a six-well plate to reach 85 to 95% confluency. The culture medium was then replaced with serum-free media with or without ORMs (40 mg/ml). After 24-hour incubation under 1% O_2, the cells were lysed, and the ATP content was measured by an ATP assay kit as per the manufacturer's instruction ($n = 3$; MilliporeSigma).

Endothelial tube formation

HAECs were cultured in a 3D collagen model described previously (*28*). Briefly, the model was prepared by mixing rat tail collagen type I (Corning), FBS, DMEM, and NaOH. A total of 400 μl of the mixture was placed in a 48-well plate and incubated at 37°C for 30 min to allow the formation of jelly-like solid collagen gel. HAECs were encapsulated in ROSS gel solution and injected into the collagen-based 3D model at a density of 10,000 cells per well. After overnight hypoxic culture, HAECs were fixed by 4% paraformaldehyde and

stained with DAPI and F-actin. Fluorescent images were taken as *z*-stacks with a confocal microscope (Zeiss LSM 700).

Implantation of hydrogel and ORMs into diabetic wounds

All animal care and experiment procedures were conducted in accordance with the National Institutes of Health guidelines. The animal protocol was approved by the Institutional Animal Care and Use Committee of Washington University in St. Louis. Eight-week old, female db/db mice (BKS.Cg-Dock7m +/+ Leprdb/J) were purchased from the Jackson laboratory. Blood glucose was measured before surgery to ensure that the glucose level was higher than 300 mg/dl. After anesthetization and removal of hair, two full-thickness, 5-mm-diameter wounds on the dorsal skin were created for each mouse using a biopsy punch. The hydrogel (6 wt% in DPBS) or Gel/ORM (6 wt% in DPBS, microspheres at 40 mg/ml) was topically administrated. Digital images of the wounds ($n \geq 8$ for each group) were taken every other day, and the wound size was determined using ImageJ. After 8 and 16 days of implantation, the mice were euthanized. The wound tissues were collected for histological and immunofluorescence analysis and RNA and protein isolation.

Histological and immunofluorescence analyses

The wound tissues were fixed in 4% paraformaldehyde overnight, embedded in paraffin, and serially sectioned at 5 μm. Hematoxylin and eosin staining was performed to measure the epidermal thickness in wounded skin. Epidermal thickness was calculated in the wound closed region. Picrosirius red staining was used to quantify the collagen deposition and collagen I/III ratio. For immunofluorescence analysis, following deparaffinization, antigen retrieval, and blocking, the sections were incubated with primary antibodies, including rabbit monoclonal anti–cytokeratin 10 (K10; Abcam, ab76318), mouse monoclonal anti–cytokeratin 14 (K14; Abcam, ab7800), rabbit monoclonal anti-CD86 (Abcam, ab234401), rat monoclonal anti-Ki67 (Invitrogen, SolA15), isolectin GS-IB_4 (Invitrogen, I21411) (*79*), and ROS indicator (CM-H_2DCFDA; Invitrogen). The sections were then incubated with corresponding secondary antibodies. Nuclei were stained with DAPI. Quantification of the stainings was performed using ImageJ. At least six images for each group were used for the quantification.

mRNA expression in in vitro cultured cells and diabetic wounds

RNA was isolated from the in vitro cultured cells or wound tissues using TRIzol following the manufacturer's instruction. cDNA was synthesized using a high-capacity cDNA reverse transcription kit (Thermo Fisher Scientific). Gene expression was performed by real-time RT-PCR using SYBR Green (Invitrogen) and selected primer pairs (table S1). β-Actin served as a housekeeping gene. Data analysis was performed using the $\Delta\Delta C_t$ method.

Protein expression in in vitro cultured cells and diabetic wounds

Protein lysates were collected from the in vitro cultured cells or wound tissues and separated by SDS–polyacrylamide gel electrophoresis. Low fluorescence polyvinylidene difluoride membranes (Bio-Rad) were used to transfer the proteins at 4°C overnight, followed by blocking and incubation with primary antibodies at 4°C. The blots were washed with PBST (DPBS + 0.1% Tween 20) and incubated with appropriate horseradish peroxidase–conjugated secondary antibodies. Immunoblots were detected using a detection kit from Advansta and imaged using ChemiDoc XRS+ System (Bio-Rad). The primary antibodies used were anti–glyceraldehyde-3-phosphate dehydrogenase (1:4000; Abcam, ab8245), anti–HO-1 (1:500; Abcam, ab52947), anti–p-Erk1/2 (1:500; Cell Signaling Technology, #9101), and anti–t-Erk1/2 (1:1000; Cell Signaling Technology, #4695).

For protein array assay, wounded tissue lysates were collected and tested using Proteome profiler mouse cytokine array kit (R&D Systems) according to the manufacturer's instructions. The pixel density was quantified using Image Lab software (Bio-Rad) (*80*).

Statistical analysis

All data were presented as means ± SD. Statistical analysis was performed between groups using one-way analysis of variance (ANOVA) with Tukey's post hoc test. A value of $P < 0.05$ was considered statistically significant.

SUPPLEMENTARY MATERIALS

Supplementary material for this article is available at http://advances.sciencemag.org/cgi/content/full/7/35/eabj0153/DC1

View/request a protocol for this paper from *Bio-protocol*.

REFERENCES AND NOTES

1. Centers for Disease Control and Prevention, in *National Diabetes Statistics Report 2020. Estimates of diabetes and its burden in the United States 2020* (Centers for Disease Control and Prevention, 2020), pp. 1–32.
2. N. Singh, D. G. Armstrong, B. A. Lipsky, Preventing foot ulcers in patients with diabetes. *JAMA* **293**, 217–228 (2005).
3. E. Everett, N. Mathioudakis, Update on management of diabetic foot ulcers. *Ann. N. Y. Acad. Sci.* **1411**, 153–165 (2018).
4. F. Gottrup, J. Apelqvist, Present and new techniques and devices in the treatment of DFU: A critical review of evidence. *Diabetes Metab. Res. Rev.* **28**, 64–71 (2012).
5. V. Falanga, Wound healing and its impairment in the diabetic foot. *Lancet* **366**, 1736–1743 (2005).
6. W. X. Hong, M. S. Hu, M. Esquivel, G. Y. Liang, R. C. Rennert, A. McArdle, K. J. Paik, D. Duscher, G. C. Gurtner, H. P. Lorenz, M. T. Longaker, The role of hypoxia-inducible factor in wound healing. *Adv. Wound Care* **3**, 390–399 (2014).
7. J. Dissemond, K. Kröger, M. Storck, A. Risse, P. Engels, Topical oxygen wound therapies for chronic wounds: A review. *J. Wound Care* **24**, 53–63 (2015).
8. G. M. Gordillo, C. K. Sen, Revisiting the essential role of oxygen in wound healing. *Am. J. Surgery* **186**, 259–263 (2003).
9. A. A. Tandara, T. A. Mustoe, Oxygen in wound healing—More than a nutrient. *World J. Surg.* **28**, 294–300 (2004).
10. S. Schreml, R. Szeimies, L. Prantl, S. Karrer, M. Landthaler, P. Babilas, Oxygen in acute and chronic wound healing. *Br. J. Dermatol.* **163**, 257–268 (2010).
11. A. P. Duzgun, H. Z. Satır, O. Ozozan, B. Saylam, B. Kulah, F. Coskun, Effect of hyperbaric oxygen therapy on healing of diabetic foot ulcers. *J. Foot Ankle Surg.* **47**, 515–519 (2008).
12. M. Löndahl, P. Katzman, A. Nilsson, C. Hammarlund, Hyperbaric oxygen therapy facilitates healing of chronic foot ulcers in patients with diabetes. *Diabetes Care* **33**, 998–1003 (2010).
13. Health Quality Ontario, Hyperbaric oxygen therapy for the treatment of diabetic foot ulcers: A health technology assessment. *Ont. Health Technol. Assess. Ser.* **17**, 1–142 (2017).
14. M. Kalani, G. Jörneskog, N. Naderi, F. Lind, K. Brismar, Hyperbaric oxygen (HBO) therapy in treatment of diabetic foot ulcers: Long-term follow-up. *J. Diabetes Complications* **16**, 153–158 (2002).
15. A. Berendt, Counterpoint: Hyperbaric oxygen for diabetic foot wounds is not effective. *Clin. Infect. Dis.* **43**, 193–198 (2006).
16. P. Kranke, M. H. Bennett, M. Martyn-St James, A. Schnabel, S. E. Debus, S. Weibel, Hyperbaric oxygen therapy for chronic wounds. *Cochrane Database Syst. Rev.* **2015**, CD004123 (2015).
17. M. Heyboer III, D. Sharma, W. Santiago, N. McCulloch, Hyperbaric oxygen therapy: Side effects defined and quantified. *Adv. Wound Care* **6**, 210–224 (2017).
18. C. Plafki, P. Peters, M. Almeling, W. Welslau, R. Busch, Complications and side effects of hyperbaric oxygen therapy. *Aviat. Space Environ. Med.* **71**, 119–124 (2000).
19. T. E. Wright, W. G. Payne, F. Ko, D. Ladizinsky, N. Bowlby, R. Neeley, B. Mannari, M. C. Robson, The effects of an oxygen-generating dressing on tissue infection and wound healing. *J. Appl. Res.* **3**, 363–370.8 (2003).

20. P. K. Chandra, C. L. Ross, L. C. Smith, S. S. Jeong, J. Kim, J. J. Yoo, B. S. Harrison, Peroxide-based oxygen generating topical wound dressing for enhancing healing of dermal wounds. *Wound Repair Regen.* **23**, 830–841 (2015).
21. P. A. Shiekh, A. Singh, A. Kumar, Exosome laden oxygen releasing antioxidant and antibacterial cryogel wound dressing OxOBand alleviate diabetic and infectious wound healing. *Biomaterials* **249**, 120020 (2020).
22. A. Wijekoon, N. Fountas-Davis, N. D. Leipzig, Fluorinated methacrylamide chitosan hydrogel systems as adaptable oxygen carriers for wound healing. *Acta Biomater.* **9**, 5653–5664 (2013).
23. D. E. Eisenbud, Oxygen in wound healing: Nutrient, antibiotic, signaling molecule, and therapeutic agent. *Clin. Plast. Surg.* **39**, 293–310 (2012).
24. A. Perez-Favila, M. L. Martinez-Fierro, J. G. Rodriguez-Lazalde, M. A. Cid-Baez, M. d. J. Zamudio-Osuna, M. Martinez-Blanco, F. E. Mollinedo-Montaño, I. P. Rodriguez-Sanchez, R. Castañeda-Miranda, I. Garza-Veloz, Current therapeutic strategies in diabetic foot ulcers. *Medicina* **55**, 714 (2019).
25. E. A. Kamoun, E.-R. S. Kenawy, X. Chen, A review on polymeric hydrogel membranes for wound dressing applications: PVA-based hydrogel dressings. *J. Adv. Res.* **8**, 217–233 (2017).
26. G. Buonocore, S. Perrone, M. L. Tataranno, in *Seminars in Fetal and Neonatal Medicine* (Elsevier, 2010), vol. 15, pp. 186–190.
27. D. Baltzis, I. Eleftheriadou, A. Veves, Pathogenesis and treatment of impaired wound healing in diabetes mellitus: New insights. *Adv. Ther.* **31**, 817–836 (2014).
28. D. Knighton, I. Silver, T. Hunt, Regulation of wound-healing angiogenesis-effect of oxygen gradients and inspired oxygen concentration. *Surgery* **90**, 262–270 (1981).
29. J. Bacon, J. Demas, Determination of oxygen concentrations by luminescence quenching of a polymer-immobilized transition-metal complex. *Anal. Chem.* **59**, 2780–2785 (1987).
30. H. M. Kimmel, A. Grant, J. Ditata, The presence of oxygen in wound healing. *Wounds* **28**, 264–270 (2016).
31. A. Cossu, A. M. Posadino, R. Giordo, C. Emanueli, A. M. Sanguinetti, A. Piscopo, M. Poiana, G. Capobianco, A. Piga, G. Pintus, Apricot melanoidins prevent oxidative endothelial cell death by counteracting mitochondrial oxidation and membrane depolarization. *PLOS ONE* **7**, e48817 (2012).
32. D. M. Castilla, Z.-J. Liu, O. C. Velazquez, Oxygen: Implications for wound healing. *Adv. Wound Care* **1**, 225–230 (2012).
33. E. J. Battegay, J. Rupp, L. Iruela-Arispe, E. H. Sage, M. Pech, PDGF-BB modulates endothelial proliferation and angiogenesis in vitro via PDGF beta-receptors. *J. Cell Biol.* **125**, 917–928 (1994).
34. X. Fan, S. Krieg, C. J. Kuo, S. J. Wiegand, M. Rabinovitch, M. L. Druzin, R. M. Brenner, L. C. Giudice, N. R. Nayak, VEGF blockade inhibits angiogenesis and reepithelialization of endometrium. *FASEB J.* **22**, 3571–3580 (2008).
35. K. E. Johnson, T. A. Wilgus, Vascular endothelial growth factor and angiogenesis in the regulation of cutaneous wound repair. *Adv. Wound Care* **3**, 647–661 (2014).
36. S. Akita, K. Akino, A. Hirano, Basic fibroblast growth factor in scarless wound healing. *Adv. Wound Care* **2**, 44–49 (2013).
37. T. M. Honnegowda, P. Kumar, E. G. P. Udupa, S. Kumar, U. Kumar, P. Rao, Role of angiogenesis and angiogenic factors in acute and chronic wound healing. *Plast. Aesthet. Res.* **2**, 243–249 (2015).
38. T. S. Kang, G. K. Gorti, S. Y. Quan, M. Ho, R. J. Koch, Effect of hyperbaric oxygen on the growth factor profile of fibroblasts. *Arch. Facial Plast. Surg.* **6**, 31–35 (2004).
39. A. Rothfuss, P. Radermacher, G. Speit, Involvement of heme oxygenase-1 (HO-1) in the adaptive protection of human lymphocytes after hyperbaric oxygen (HBO) treatment. *Carcinogenesis* **22**, 1979–1985 (2001).
40. C. Dennog, P. Radermacher, Y. A. Barnett, G. Speit, Antioxidant status in humans after exposure to hyperbaric oxygen. *Mutat. Res.* **428**, 83–89 (1999).
41. F. Anjum, N. A. Agabalyan, H. D. Sparks, N. L. Rosin, M. S. Kallos, J. Biernaskie, Biocomposite nanofiber matrices to support ECM remodeling by human dermal progenitors and enhanced wound closure. *Sci. Rep.* **7**, 10291 (2017).
42. M. Tong, B. Tuk, P. Shang, I. M. Hekking, E. M. Fijneman, M. Guijt, S. E. Hovius, J. W. van Neck, Diabetes-impaired wound healing is improved by matrix therapy with heparan sulfate glycosaminoglycan mimetic OTR4120 in rats. *Diabetes* **61**, 2633–2641 (2012).
43. A. D. Widgerow, Cellular/extracellular matrix cross-talk in scar evolution and control. *Wound Repair Regen.* **19**, 117–133 (2011).
44. S. Rius-Pérez, I. Torres-Cuevas, I. Millán, Á. L. Ortega, S. Pérez, PGC-1α, inflammation, and oxidative stress: An integrative view in metabolism. *Oxid. Med. Cell. Longev.* **2020**, 1–20 (2020).
45. H. Bitterman, Bench-to-bedside review: Oxygen as a drug. *Crit. Care* **13**, 205 (2009).
46. A. Gupta, R. Raghubir, Energy metabolism in the granulation tissue of diabetic rats during cutaneous wound healing. *Mol. Cell. Biochem.* **270**, 71–77 (2005).
47. G. Han, R. Ceilley, Chronic wound healing: A review of current management and treatments. *Adv. Ther.* **34**, 599–610 (2017).
48. H. Chen, Y. Cheng, J. Tian, P. Yang, X. Zhang, Y. Chen, Y. Hu, J. Wu, Dissolved oxygen from microalgae-gel patch promotes chronic wound healing in diabetes. *Sci. Adv.* **6**, eaba4311 (2020).
49. Z. Li, X. Guo, A. F. Palmer, H. Das, J. Guan, High-efficiency matrix modulus-induced cardiac differentiation of human mesenchymal stem cells inside a thermosensitive hydrogel. *Acta Biomater.* **8**, 3586–3595 (2012).
50. Z. Fan, Z. Xu, H. Niu, N. Gao, Y. Guan, C. Li, Y. Dang, X. Cui, X. L. Liu, Y. Duan, H. Li, X. Zhou, P.-H. Lin, J. Ma, J. Guan, An injectable oxygen release system to augment cell survival and promote cardiac repair following myocardial infarction. *Sci. Rep.* **8**, 1371 (2018).
51. S. E. Bae, J. S. Son, K. Park, D. K. Han, Fabrication of covered porous PLGA microspheres using hydrogen peroxide for controlled drug delivery and regenerative medicine. *J. Control. Release* **133**, 37–43 (2009).
52. S.-M. Ng, J.-Y. Choi, H.-S. Han, J.-S. Huh, J. O. Lim, Novel microencapsulation of potential drugs with low molecular weight and high hydrophilicity: Hydrogen peroxide as a candidate compound. *Int. J. Pharm.* **384**, 120–127 (2010).
53. J. Michaels, S. S. Churgin, K. M. Blechman, M. R. Greives, S. Aarabi, R. D. Galiano, G. C. Gurtner, db/db mice exhibit severe wound-healing impairments compared with other murine diabetic strains in a silicone-splinted excisional wound model. *Wound Repair Regen.* **15**, 665–670 (2007).
54. P. Sheffield, Measuring tissue oxygen tension: A review. *Undersea Hyperb. Med.* **25**, 179–188 (1998).
55. A. Sendoel, M. O. Hengartner, Apoptotic cell death under hypoxia. *Phys. Ther.* **29**, 168–176 (2014).
56. L. M. Wise, M. K. Inder, N. C. Real, G. S. Stuart, S. B. Fleming, A. A. Mercer, The vascular endothelial growth factor (VEGF)-E encoded by orf virus regulates keratinocyte proliferation and migration and promotes epidermal regeneration. *Cell. Microbiol.* **14**, 1376–1390 (2012).
57. M. A. Seeger, A. S. Paller, The roles of growth factors in keratinocyte migration. *Adv. Wound Care* **4**, 213–224 (2015).
58. S. Barrientos, O. Stojadinovic, M. S. Golinko, H. Brem, M. Tomic-Canic, Growth factors and cytokines in wound healing. *Wound Repair Regen.* **16**, 585–601 (2008).
59. N. W. DeLapp, D. K. Dieckman, Effect of basic fibroblast growth factor (bFGF) and insulin-like growth factors type I (IGF-I) and type II (IGF-II) on adult human keratinocyte growth and fibronectin secretion. *J. Invest. Dermatol.* **94**, 777–780 (1990).
60. D. Carbonari, A. Campopiano, D. Ramires, E. Strafella, S. Staffolani, M. Tomasetti, R. Curini, M. Valentino, L. Santarelli, M. Amati, Angiogenic effect induced by mineral fibres. *Toxicology* **288**, 34–42 (2011).
61. C. Spirli, S. Okolicsanyi, R. Fiorotto, L. Fabris, M. Cadamuro, S. Lecchi, X. Tian, S. Somlo, M. Strazzabosco, ERK1/2-dependent vascular endothelial growth factor signaling sustains cyst growth in polycystin-2 defective mice. *Gastroenterology* **138**, 360–371.e7 (2010).
62. Y. An, W. J. Liu, P. Xue, Y. Ma, L. Q. Zhang, B. Zhu, M. Qi, L. Y. Li, Y. J. Zhang, Q. T. Wang, Y. Jin, Autophagy promotes MSC-mediated vascularization in cutaneous wound healing via regulation of VEGF secretion. *Cell Death Dis.* **9**, 58 (2018).
63. Q.-Y. Chen, G.-G. Wang, W. Li, Y.-X. Jiang, X.-H. Lu, P.-P. Zhou, Heme oxygenase-1 promotes delayed wound healing in diabetic rats. *J. Diabetes Res.* **2016**, 1–10 (2016).
64. A. Grochot-Przeczek, R. Lach, J. Mis, K. Skrzypek, M. Gozdecka, P. Sroczynska, M. Dubiel, A. Rutkowski, M. Kozakowska, A. Zagorska, J. Walczynski, H. Was, J. Kotlinowski, J. Drukala, K. Kurowski, C. Kieda, Y. Herault, J. Dulak, A. Jozkowicz, Heme oxygenase-1 accelerates cutaneous wound healing in mice. *PLOS ONE* **4**, e5803 (2009).
65. J. J. Salazar, W. J. Ennis, T. J. Koh, Diabetes medications: Impact on inflammation and wound healing. *J. Diabetes Complications* **30**, 746–752 (2016).
66. P. Mohanty, W. HAmouda, R. Garg, A. Aljada, H. Ghanim, P. Dandona, Glucose challenge stimulates reactive oxygen species (ROS) generation by leucocytes. *J. Clin. Endocrinol. Metabol.* **85**, 2970–2973 (2000).
67. A. Saaristo, T. Tammela, A. Färkkilä, M. Kärkkäinen, E. Suominen, S. Yla-Herttuala, K. Alitalo, Vascular endothelial growth factor-C accelerates diabetic wound healing. *Am. J. Pathol.* **169**, 1080–1087 (2006).
68. Y. Zheng, M. Watanabe, T. Kuraishi, S. Hattori, C. Kai, M. Shibuya, Chimeric VEGF-ENZ7/PlGF specifically binding to VEGFR-2 accelerates skin wound healing via enhancement of neovascularization. *Arterioscler. Thromb. Vasc. Biol.* **27**, 503–511 (2007).
69. S. Wood, V. Jayaraman, E. J. Huelsmann, B. Bonish, D. Burgad, G. Sivaramakrishnan, S. Qin, L. A. DiPietro, A. Zloza, C. Zhang, S. H. Shafikhani, Pro-inflammatory chemokine CCL2 (MCP-1) promotes healing in diabetic wounds by restoring the macrophage response. *PLOS ONE* **9**, e91574 (2014).
70. S. E. Navone, L. Pascucci, M. Dossena, A. Ferri, G. Invernici, F. Acerbi, S. Cristini, G. Bedini, V. Tosetti, V. Ceserani, A. Bonomi, A. Pessina, G. Freddi, A. Alessandrino, P. Ceccarelli, R. Campanella, G. Marfia, G. Alessandri, E. A. Parati, Decellularized silk fibroin scaffold primed with adipose mesenchymal stromal cells improves wound healing in diabetic mice. *Stem Cell Res. Ther.* **5**, 7 (2014).
71. L. Liu, G. P. Marti, X. Wei, X. Zhang, H. Zhang, Y. V. Liu, M. Nastai, G. L. Semenza, J. W. Harmon, Age-dependent impairment of HIF-1α expression in diabetic mice:

Correction with electroporation-facilitated gene therapy increases wound healing, angiogenesis, and circulating angiogenic cells. *J. Cell. Physiol.* **217**, 319–327 (2008).
72. C.-C. Song, R. Ji, F.-S. Du, D.-H. Liang, Z.-C. Li, Oxidation-accelerated hydrolysis of the ortho ester-containing acid-labile polymers. *ACS Macro Lett.* **2**, 273–277 (2013).
73. H. Niu, X. Li, H. Li, Z. Fan, J. Ma, J. Guan, Thermosensitive, fast gelling, photoluminescent, highly flexible, and degradable hydrogels for stem cell delivery. *Acta Biomater.* **83**, 96–108 (2019).
74. Y. Guan, H. Niu, Y. Dang, N. Gao, J. Guan, Photoluminescent oxygen-release microspheres to image the oxygen release process in vivo. *Acta Biomater.* **115**, 333–342 (2020).
75. J. Li, Y. Shu, T. Hao, Y. Wang, Y. Qian, C. Duan, H. Sun, Q. Lin, C. Wang, A chitosan–glutathione based injectable hydrogel for suppression of oxidative stress damage in cardiomyocytes. *Biomaterials* **34**, 9071–9081 (2013).
76. Y. Zhu, Y. Matsumura, M. Velayutham, L. M. Foley, T. K. Hitchens, W. R. Wagner, Reactive oxygen species scavenging with a biodegradable, thermally responsive hydrogel compatible with soft tissue injection. *Biomaterials* **177**, 98–112 (2018).
77. Y. Guan, N. Gao, H. Niu, Y. Dang, J. Guan, Oxygen-release microspheres capable of releasing oxygen in response to environmental oxygen level to improve stem cell survival and tissue regeneration in ischemic Hindlimbs. *J. Control. Release* **331**, 376–389 (2021).
78. H. Niu, C. Li, Y. Guan, Y. Dang, X. Li, Z. Fan, J. Shen, L. Ma, J. Guan, High oxygen preservation hydrogels to augment cell survival under hypoxic condition. *Acta Biomater.* **105**, 56–67 (2020).
79. W. Dong, R. Li, H. Yang, Y. Lu, L. Zhou, L. Sun, D. Wang, J. Duan, Mesenchymal-endothelial transition-derived cells as a potential new regulatory target for cardiac hypertrophy. *Sci. Rep.* **10**, 6652 (2020).
80. J. E. Gilda, A. V. Gomes, Stain-Free total protein staining is a superior loading control to β-actin for Western blots. *Anal. Biochem.* **440**, 186–188 (2013).

Acknowledgments: Confocal images were performed, in part, through the use of the Washington University Center for Cellular Imaging (WUCCI) supported by Washington University School of Medicine, The Children's Discovery Institute of Washington University and St. Louis Children's Hospital (CDI-CORE-2015-505 and CDI-CORE-2019-813), and the Foundation for Barnes-Jewish Hospital (3770 and 4642). We thank the Musculoskeletal Research Center in Washington University School of Medicine for help with histological sections. We thank M. Singh from the Department of Chemistry in Washington University for help with EPR test. We thank InPrint and J. Ballard from the Engineering Communication Center in Washington University for editing the manuscript. **Funding:** This work was supported by NIH (R01HL138175, R01HL138353, R01EB022018, R01AG056919, R01AR077616, R01AR075860, and R21AR077226) and NSF (1922857). **Author contributions:** J.G., Y.G., and H.N. designed the study. Y.G., H.N., and Z.L. performed most of the experiments. J.G., Y.G., H.N., and Y.D. analyzed the results and wrote the manuscript. M.Z., L.M., and J.S. provided insights of the study and edited the manuscript. J.G. supervised the project. **Competing interests:** The authors declare that they have no competing interests. **Data and materials availability:** All data needed to evaluate the conclusions in the paper are present in the paper and/or the Supplementary Materials.

Submitted 14 April 2021
Accepted 6 July 2021
Published 27 August 2021
10.1126/sciadv.abj0153

Citation: Y. Guan, H. Niu, Z. Liu, Y. Dang, J. Shen, M. Zayed, L. Ma, J. Guan, Sustained oxygenation accelerates diabetic wound healing by promoting epithelialization and angiogenesis and decreasing inflammation. *Sci. Adv.* **7**, eabj0153 (2021).

ScienceAdvances

Sustained oxygenation accelerates diabetic wound healing by promoting epithelialization and angiogenesis and decreasing inflammation

Ya GuanHong NiuZhongting LiuYu DangJie ShenMohamed ZayedLiang MaJianjun Guan

Sci. Adv., 7 (35), eabj0153.

Science Advances (ISSN) is published by the American Association for the Advancement of Science. 1200 New York Avenue NW, Washington, DC 20005. The title *Science Advances* is a registered trademark of AAAS.